Deceleration of a Finite-Width, Stratified Current over a Sloping Bottom: Frictional Spindown or Buoyancy Shutdown?*

DAVID C. CHAPMAN

Woods Hole Oceanographic Institution, Woods Hole, Massachusetts

(Manuscript received 23 October 2000, in final form 3 July 2001)

ABSTRACT

The deceleration of an unforced, two-dimensional, finite-width current over a sloping bottom in a stratified fluid is studied to quantify the relative importance of frictional spindown and buoyancy shutdown when both act simultaneously. Frictional spindown decelerates the current through Ekman suction and pumping at the current edges, which transmit stresses into the interior fluid. Buoyancy shutdown is the process by which lateral advection of density in the bottom boundary layer generates thermal wind shears that reduce the bottom stress, thereby halting deceleration.

A theoretical model of a downwelling current suggests that buoyancy shutdown always reduces the deceleration timescale from that for frictional spindown alone and produces a nonzero steady along-isobath current overlying an arrested bottom mixed layer. The model is most sensitive to the Burger number $S = N\alpha/f$ where N is the buoyancy frequency, α the bottom slope, and f the Coriolis parameter. Larger S produces a stronger steady current that is reached more rapidly. Buoyancy shutdown remains important in the deceleration process even when its individual timescale for adjustment is an order of magnitude longer than the frictional spindown timescale. The model suggests that buoyancy shutdown should influence currents over the continental shelf on timescales of about five days and greater.

A primitive-equation numerical model is used to test the theory and its assumptions. Overall, the results are supportive of the theory, except that the theoretical model neglects the cross-isobath component of bottom stress and ignores vertical shears above the bottom mixed layer. As a result, the numerical model current initially decelerates more slowly and then continues to decelerate after the along-isobath stress has vanished, leaving a weaker steady flow, especially with stronger stratification. Interior vertical shears in the numerical model tend to decouple the near-surface flow from the bottom mixed layer, producing more variable steady flows. Details of the flow in the bottom mixed layer are highly dependent on the choice of turbulence closure scheme.

Buoyancy shutdown is also important in the deceleration of upwelling currents, substantially reducing the time to reach steady state from that for frictional spindown alone. Details of both the deceleration and the steady state vary sharply with the turbulent closure scheme, so generalizations are difficult.

1. Introduction

The response of any dynamical system to changes in forcing depends critically on the damping of the system. A classic example is the damped harmonic oscillator, which can relax to equilibrium with either a gradually decaying oscillation or a purely exponential decay, depending on the magnitude of frictional damping. Ocean currents are no exception, and an improved understanding of the damping or deceleration of ocean currents should lead to a better understanding of the timescales of their response to variable driving forces and their relaxation following the cessation of forcing.

Deceleration is basically a frictional effect primarily caused by contact of a current with the bottom and the subsequent generation of a bottom Ekman layer. Lateral variations in the current, for example, at the edges of the current, cause Ekman suction and pumping through the top of the Ekman layer, thereby communicating the bottom stress to the fluid above and slowing the entire current. This is the classic *frictional spindown* process. The vertical velocities introduced by Ekman suction and pumping are necessary for frictional spindown; for example, an initially uniform current without horizontal limits would not produce Ekman suction or pumping and thus would not decelerate.

Stratification and a sloping bottom complicate the dynamics of the deceleration process because the bottom Ekman layer can redistribute buoyancy (i.e., density) and introduce vertical shears in the current that, in turn, can reduce the bottom stress. Reduced bottom stress then leads to slower spindown of the overlying flow, and possibly a situation in which bottom stress vanishes

* Woods Hole Oceanographic Institution Contribution Number 10361.

Corresponding author address: David Chapman, Woods Hole Oceanographic Institution, Woods Hole, MA 02543.
E-mail: dchapman@whoi.edu

and the deceleration of the overlying flow stops entirely. Such an Ekman layer is said to have been arrested by a process that may be called *buoyancy shutdown.* [For details, see the review by Garrett et al. (1993) and more recent papers by Ramsden (1995a,b) and Middleton and Ramsden (1996).]

Frictional spindown and buoyancy shutdown have primarily been studied separately, yet the potential for strong coupling and feedback between the two processes when acting simultaneously is clear. Garrett et al. (1993) have speculated on the relative importance of each process based on estimates of their respective timescales. For example, frictional spindown of an unstratified flow (no buoyancy shutdown) acts on a timescale

$$T_F = h/r, \tag{1}$$

where h is the water depth and r is a linear bottom friction coefficient (e.g., Pedlosky 1987). Buoyancy shutdown alone acts on a timescale estimated by Garrett et al. (1993) to be

$$T_B = \left(\frac{f}{\alpha N}\right)^3 \frac{U}{rN}, \tag{2}$$

where N is the initial buoyancy frequency, α the bottom slope, f the Coriolis parameter, and U the velocity scale of the current. (Note that linear bottom drag has been used here, where $r = C_D U$ and C_D is a drag coefficient.) When both processes act simultaneously, the process with the shorter timescale presumably dominates. That is, if $T_F < T_B$, then buoyancy shutdown may not have enough time to significantly alter the current before it is halted by frictional spindown. If $T_B < T_F$, then bottom stress may vanish before the current has been slowed by frictional spindown, hardly changing the overlying flow. However, simply comparing timescales does not take into account the coupling and feedback between the processes. The individual timescales may, in fact, be inappropriate for the combined effect of both processes. Furthermore, T_B and therefore the size of T_B relative to T_F are highly sensitive to the buoyancy frequency (N^{-4}) and bottom slope (α^{-3}), suggesting that application to ocean currents may be difficult.

To address these issues, I present in section 2 a theoretical model in which both frictional spindown and buoyancy shutdown act simultaneously on a decelerating current. In order to obtain an analytical solution, only downwelling flows are considered (shallow water on the right looking downstream in the Northern Hemisphere), and numerous simplifications are made. The theory and assumptions are then tested in section 3 using a primitive-equation numerical model with more complete dynamics. The numerical model is also used to examine briefly the deceleration of upwelling flows. Some discussion and conclusions follow in sections 4 and 5, respectively.

It should be pointed out that the basic theoretical approach taken here is close to that of Chapman and Lentz (1997), who studied the three-dimensional adjustment of a steady stratified flow over a sloping bottom. In their case, the coupling of frictional spreading (rather than spindown) with buoyancy shutdown produced a downstream equilibrium, conceptually equivalent to the present steady state. However, the lateral spreading of the flow in three-dimensions is a fundamental difference from the present problem (see below), and apparently precludes a simple transformation between the two problems. Thus, Chapman and Lentz (1997) were unable to find an analytical solution.

2. Theoretical model

a. Formulation

I consider the deceleration of an unforced, initially depth-independent, uniform current u_0 with finite width, flowing along a sloping bottom in a stratified fluid (Fig. 1a). The flow is assumed hydrostatic and two-dimensional with no variations along the isobaths (x direction). The along-isobath velocity is assumed to be in geostrophic balance throughout the water column at all times. Advection of momentum is assumed negligible, but advection of density is included. With these assumptions, the equations of motion are

$$u_t - fv = \tau^x_z/\rho_0 \tag{3}$$

$$fu = -p_y/\rho_0 \tag{4}$$

$$0 = p_z + g\rho \tag{5}$$

$$v_y + w_z = 0 \tag{6}$$

$$\rho_t + v\rho_y + w\rho_z = D_z, \tag{7}$$

where (u, v, w) are the velocity components in the along-isobath (x), cross-isobath (y), and vertical (z) directions, respectively; p is pressure; ρ is the density anomaly relative to the constant surface density ρ_0; f is the Coriolis parameter; τ^x is the stress in the x direction; D is the vertical turbulent density flux; and g is gravitational acceleration. Subscripts y, z, and t denote partial differentiation. For convenience, the density anomaly ρ is referred to as the density.

The surface ($z = 0$) is assumed rigid, so (6) may be integrated vertically from the bottom at $z = -h(y)$ to the surface to obtain $(\int_{-h}^{0} v\, dz)_y = 0$. Since $v = 0$ beyond the edges of the current (Fig. 1a), then $\int_{-h}^{0} v\, dz = 0$ everywhere. This means that the current width does not change during the deceleration process, and the flow may be considered locally one-dimensional, with the water column along each isobath decelerating independently. Thus, u depends on y only parametrically through the depth h.

As the flow begins to decelerate, a bottom Ekman layer forms that transports density downslope for $u_0 > 0$ or upslope for $u_0 < 0$. In the downwelling case, lighter water is carried under denser water, which, being unstable, mixes rapidly in the vertical to create a thick

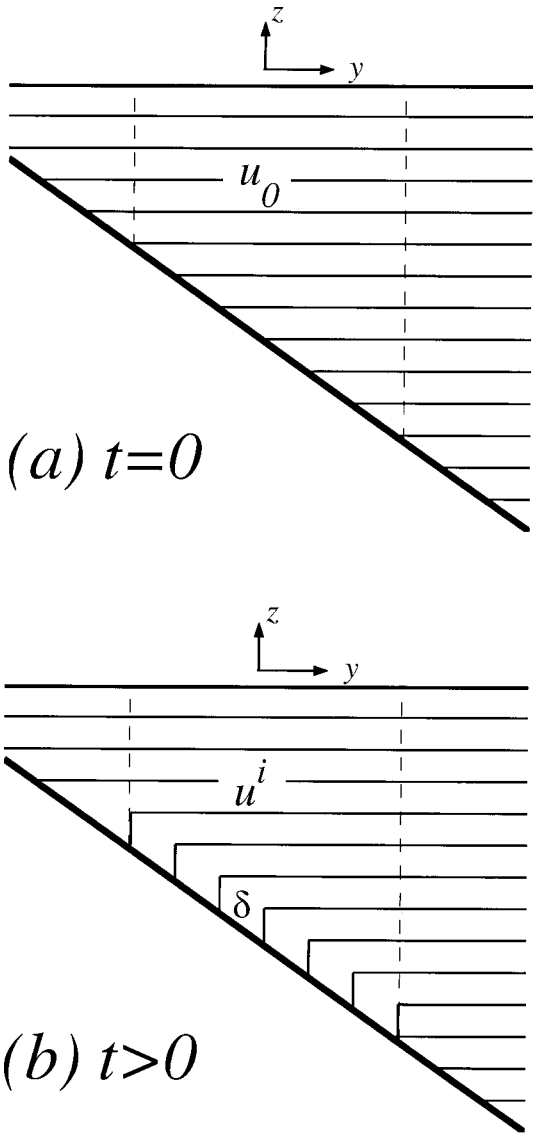

FIG. 1. Theoretical model geometry and stratification for (a) the initial condition and (b) later times. The initial current u_0 is uniform between the vertical dashed lines. During deceleration, the interior velocity u^i is assumed depth independent above a bottom mixed layer with thickness δ.

boundary layer with vertically uniform density that can extend well above the bottom Ekman layer. I call this the *bottom mixed layer* to distinguish it from the Ekman layer. Note that the Ekman layer is always present, but the bottom mixed layer can only exist in a stratified fluid (unless one considers it to extend through the entire water column in an unstratified fluid).

The resulting flow at later times consists of two regions (Fig. 1b), an interior with vertically uniform velocity u^i and the bottom mixed layer with thickness δ. Of course, this cannot be strictly true near the edges of the current where Ekman suction and pumping generate strong vertical velocities, but it should be a reasonable approximation away from the edges. The along-isobath velocity in the bottom mixed layer can be found by vertically integrating the thermal wind balance [$u_z = g\rho_y/\rho_0 f$ from (4) and (5)] and noting that ρ_y is independent of z in the bottom mixed layer:

$$u = u^i - \frac{g}{\rho_0 f}\rho_y(\delta - h - z), \qquad -h \le z \le -h + \delta. \tag{8}$$

For uniform stratification

$$\rho = -\rho_0 N^2 z/g, \tag{9}$$

and (8) can be written

$$u = u^i - \frac{\alpha N^2}{f}(\delta - h - z), \qquad -h \le z \le -h + \delta, \tag{10}$$

where α is the bottom slope and δ is assumed independent of y. The latter amounts to assuming that the bottom mixed layer grows uniformly beneath the current.

An equation for u^i can be found by substituting (10) into the x-momentum equation (3), integrating vertically from the bottom to the surface, noting that $\int_{-h}^{0} v\, dz = 0$ everywhere, and assuming a linear bottom drag law of the form $\tau^x = \rho_0 r u$ at $z = -h$, where r is a bottom friction coefficient. The result is

$$\frac{du^i}{dt} + \frac{r}{h}u^i = \frac{\alpha N^2}{fh}\left(\frac{1}{2}\frac{d\delta^2}{dt} + r\delta\right), \tag{11}$$

which is now an ordinary differential equation because t is effectively the only independent variable.

The density equation (7) may be integrated vertically through the bottom mixed layer to obtain an equation for δ. The vertical advection term vanishes because $\rho_z = 0$ in the bottom mixed layer. The turbulent density flux contributes nothing because there is no density flux through the bottom or into the interior (i.e., $D = 0$ at $z = -h$ and $z = -h + \delta$). I further assume that u_t is small compared to fv within the bottom mixed layer, so $v \approx -\tau_z^x/\rho_0 f$ there. This approximation is justified a posteriori by the numerical results in section 3. Making use of (9), (10) and the definition of bottom stress given above, yields

$$\frac{d\delta^2}{dt} = \frac{2\alpha r}{f}\left(u^i - \frac{\alpha N^2}{f}\delta\right). \tag{12}$$

Equations (11) and (12) form a set of coupled nonlinear ordinary differential equations for unknowns u^i and δ. Equation (11) describes the deceleration of the interior velocity as it is altered by the bottom mixed layer. Without stratification ($N = 0$), the solution of (11) is $u^i = u_0 e^{-rt/h}$; that is, the current decelerates entirely due to frictional spindown with timescale h/r as in (1). With stratification, (12) describes the bottom mixed lay-

er growth, which stops when δ becomes large enough to reduce the bottom velocity to zero; that is, $\delta = u^i f/\alpha N^2$. At this time, the steady-state limits of both (11) and (12) are satisfied, so deceleration stops. This result was obtained by Trowbridge and Lentz (1991); the difference here is that both u^i and δ are unknowns, so the steady state cannot be found a priori. In fact, there is no guarantee that this state will be reached.[1]

To simplify (11) and (12), t is scaled by the frictional spindown time h/r, u by the initial velocity u_0, and δ by the depth h. Equations (11) and (12) become, in terms of scaled variables,

$$\frac{du^i}{dt} + u^i = \frac{S^2}{\mathrm{Ro}}\left(\frac{1}{2}\frac{d\delta^2}{dt} + \delta\right) \tag{13}$$

$$\frac{d\delta^2}{dt} = 2\mathrm{Ro}\left(u^i - \frac{S^2}{\mathrm{Ro}}\delta\right), \tag{14}$$

where $S = N\alpha/f$ is the Burger number and $\mathrm{Ro} = u_0\alpha/fh$ is a Rossby number. A single equation for u^i is obtained by first substituting (14) into (13) and rewriting as

$$\frac{du^i}{dt} = -(1 - S^2)\left(u^i - \frac{S^2}{\mathrm{Ro}}\delta\right). \tag{15}$$

Then, equating the terms in the large brackets on the right-hand sides of (14) and (15), and integrating in time produces

$$\delta = \left(\frac{2\mathrm{Ro}}{1 - S^2}\right)^{1/2}(1 - u^i)^{1/2}, \tag{16}$$

which may be substituted into (15) to obtain

$$\frac{du^i}{dt} = \left[2(1 - S^2)\frac{S^4}{\mathrm{Ro}}\right]^{1/2}(1 - u^i)^{1/2} - (1 - S^2)u^i. \tag{17}$$

The constant of integration in (16) has been chosen to satisfy the initial condition of $\delta = 0$ and $u^i = 1$ at $t = 0$. The solution to (17), found by a change of variables and an integration, is

$$\frac{A}{(A^2 + 4B^2)^{1/2}}\log\left|\frac{2B(1 - u^i)^{1/2} + A - (A^2 + 4B^2)^{1/2}}{2B(1 - u^i)^{1/2} + A + (A^2 + 4B^2)^{1/2}}\right| - \log|B(1 - u^i) + A(1 - u^i)^{1/2} - B| = Bt + C, \tag{18}$$

where $A = [2(1 - S^2)S^4/\mathrm{Ro}]^{1/2}$, $B = (1 - S^2)$, and C is chosen to satisfy the initial condition of $u^i = 1$ at $t = 0$;

$$C = \frac{A}{(A^2 + 4B^2)^{1/2}}\log\left|\frac{A - (A^2 + 4B^2)^{1/2}}{A + (A^2 + 4B^2)^{1/2}}\right| - \log|B|.$$

The bottom mixed layer thickness δ is recovered from (16). Note that the bottom friction coefficient r does not appear in the scaled equations, having been absorbed in the scaled time.

The solution (18) depends on the two nondimensional parameters S and Ro. The assumed equations of motion (3)–(6), when combined with the scales introduced above, place restrictions on S and Ro and provide scales for v and w. For example, the neglect of the nonlinear momentum terms in (3) and (4) requires $\mathrm{Ro} \ll 1$. Equations (4) and (5) combine to produce the thermal wind balance, which holds only if $S^2 \sim \mathrm{Ro}$, so $S^2 \ll 1$ is also required. For u_t and fv to be the same order in (3), v must be scaled by $u_0 r/fh$. To have neglected v_t relative to fu in (4) then demands that $(r/fh)^2 \ll 1$. That is, the frictional spindown time h/r must be much greater than f^{-1}, which is satisfied for depths greater than about 15 m. Continuity (6) requires that w be scaled by $u_0 r\alpha/fh$.

b. Results

For typical ocean values of N, α, and f, the Burger number S is usually less than about 0.5. Choosing an initial velocity of 0.1 m s^{-1}, Ro is typically much less than one, rarely exceeding about 0.05. Figure 2 shows u^i and δ from (18) and (16) for several combinations of S and Ro. In each case, the scaled interior velocity u^i decreases from its initial value of one, smoothly approaching a steady state. The case of $S = 0$ is pure frictional spindown, for which (15) yields $u^i = e^{-t}$ with a steady state of $u^i = 0$. Strictly speaking, there is no bottom mixed layer and, hence, no thermal wind balance when $S = 0$. However, the maximum possible thickness of the bottom mixed layer occurs when $S \to 0$, and this limit can be found by setting $S = 0$ in (14), substituting $u^i = e^{-t}$, and integrating to obtain $\delta = (2\mathrm{Ro})^{1/2}(1 - e^{-t})^{1/2}$. The thin curves in Fig. 2b show this limit, approaching the steady-state value $\delta = (2\mathrm{Ro})^{1/2}$.

Stratification slows the initial deceleration because the growing bottom mixed layer rapidly reduces the bottom stress. The effect is greater for stronger stratification (larger S) and for smaller Ro. The bottom mixed layer grows much faster for larger Ro, and slightly faster for smaller S. It is important to note that, in the presence of stratification, a steady state is *always* reached with nonzero u^i. That is, buoyancy shutdown always modifies frictional spindown, regardless of the relative sizes of the individual timescales. This is discussed more below.

The steady state, found from either (17) or (18), is

$$u_s^i = \frac{S^4}{(1 - S^2)\mathrm{Ro}}\left\{\left[1 + 2(1 - S^2)\frac{\mathrm{Ro}}{S^4}\right]^{1/2} - 1\right\} \tag{19}$$

$$\delta_s = \frac{\mathrm{Ro}}{S^2}u_s^i = \frac{S^2}{1 - S^2}\left\{\left[1 + 2(1 - S^2)\frac{\mathrm{Ro}}{S^4}\right]^{1/2} - 1\right\}. \tag{20}$$

[1] As noted above, the present problem is related to that considered by Chapman and Lentz (1997). They obtained equations similar in form to (11) and (12), but their equations involved two independent variables because the current could widen as it moved downstream. This fundamental difference appears to preclude an analytical solution to their problem.

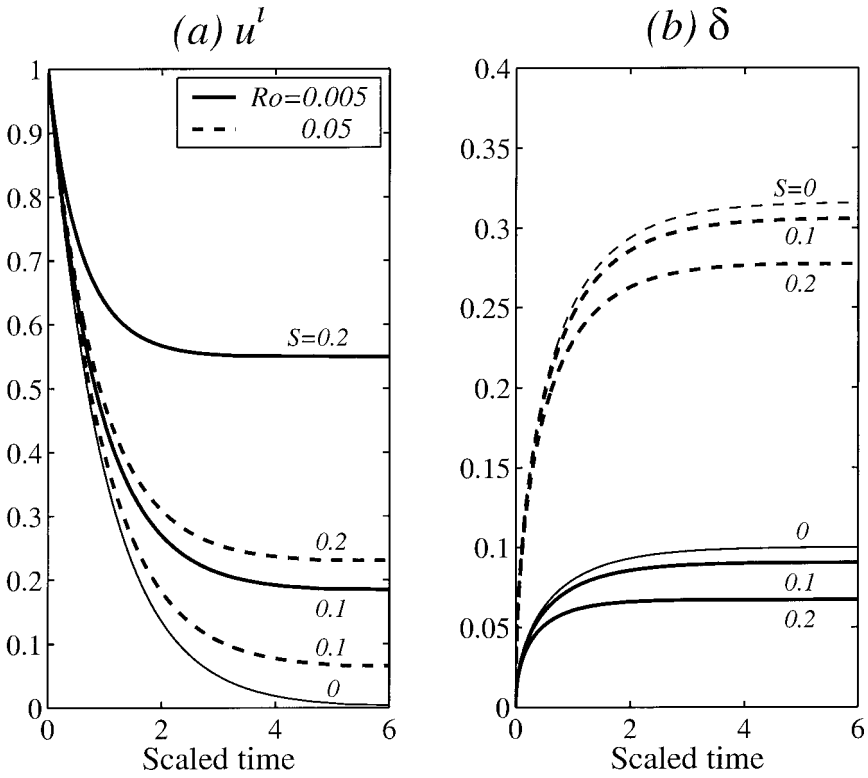

FIG. 2. Time evolution of the scaled (a) interior velocity and (b) bottom mixed layer thickness from the theoretical model with several combinations of S and Ro.

The limits of frictional spindown and buoyancy shutdown are fairly straightforward. For pure frictional spindown, $S \to 0$ and $u_s^i \to 0$ while $\delta_s \to (2\text{Ro})^{1/2}$, as noted above. For pure buoyancy shutdown, the fluid depth h is effectively infinite, so Ro $\to 0$ and a Taylor series expansion of the term in square brackets in (19) leads to $u_s^i \to 1$; that is, the interior flow does not change. According to (20), δ_s vanishes when Ro $\to 0$, but this is misleading because δ_s has been scaled by depth h, which is approaching infinity. Instead, when written in terms of unscaled variables, $u_s^i = u_0$, so $\delta_s = u_0 f/\alpha N^2$ from (12), in agreement with Trowbridge and Lentz (1991).

Figure 3 shows u_s^i and δ_s, each contoured over a range of S and Ro. From the limits discussed above, the $S = 0$ axis represents pure frictional spindown, while the Ro $= 0$ axis represents pure buoyancy shutdown. Over most of Fig. 3a (i.e., Ro > 0.005), u_s^i is relatively independent of Ro. Strong dependence on Ro appears only as Ro approaches zero, where u_s^i rapidly approaches unity for all values of S. The important point here is that S need not be large for buoyancy shutdown to significantly influence deceleration. For example, when $S = 0.2$ and Ro $= 0.005$, the current slows to 55% of its initial value and remains at this speed. The steady bottom mixed layer thickness (Fig. 3b) decreases as S increases because, with increased stratification, a thinner mixed layer provides sufficient vertical shear to reduce the interior velocity to zero at the bottom. Neither u_s^i nor δ_s depends on the bottom friction coefficient r because r appears only in the scaled time, and time dependence is absent in the steady state by definition. Physically, r affects the rate of deceleration but not the steady state.

The deceleration to steady state is not a simple exponential decay (except for pure frictional spindown), so estimates of the timescale are somewhat ad hoc. Here I define the timescale as the time needed to decay 95% of the way to steady state. This can then be compared to the time taken for frictional spindown to decay to $u^i = 0.05$ (i.e., 95%) to show the influence of buoyancy shutdown. Figure 4 shows contours of these relative timescales for the same ranges of S and Ro as in Fig. 3. By this measure, buoyancy shutdown always *reduces* the deceleration timescale from that of frictional spindown alone. That is, the flow reaches steady state sooner whenever buoyancy shutdown is active. The contours closely follow those of Fig. 3a, but with opposite tendencies. The reduction in timescale increases with increasing S and/or decreasing Ro. Again, S need not be very large for the timescale to be significantly reduced.

The steady-state solution can be recast in terms of the ratio of timescales for frictional spindown and buoyancy shutdown, which from (1) and (2) is

$$T_F/T_B = S^4/\text{Ro}, \tag{21}$$

where the initial velocity u_0 has been used for the ve-

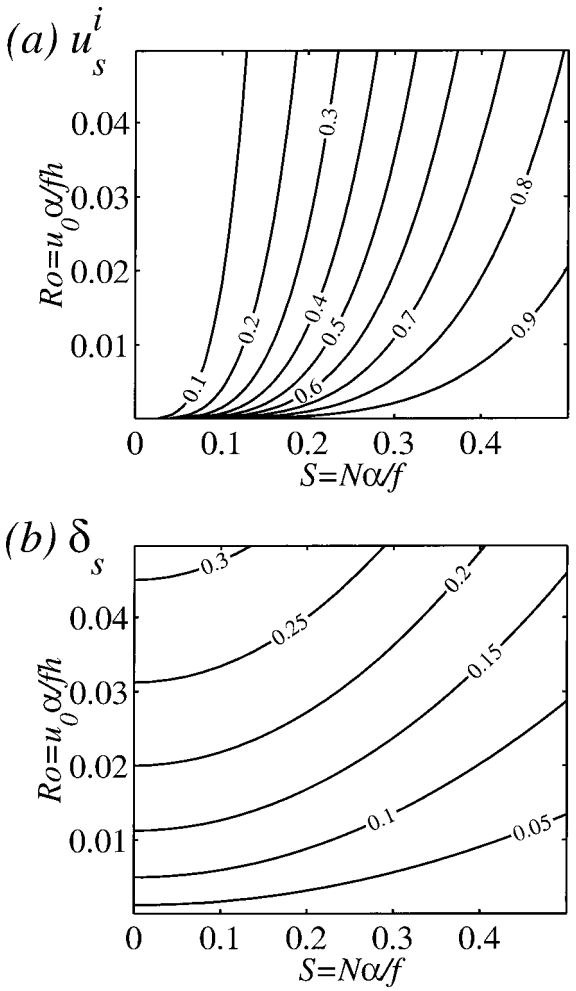

FIG. 3. Contours of steady scaled (a) interior velocity and (b) bottom mixed layer thickness from the theoretical model for a range of S and Ro.

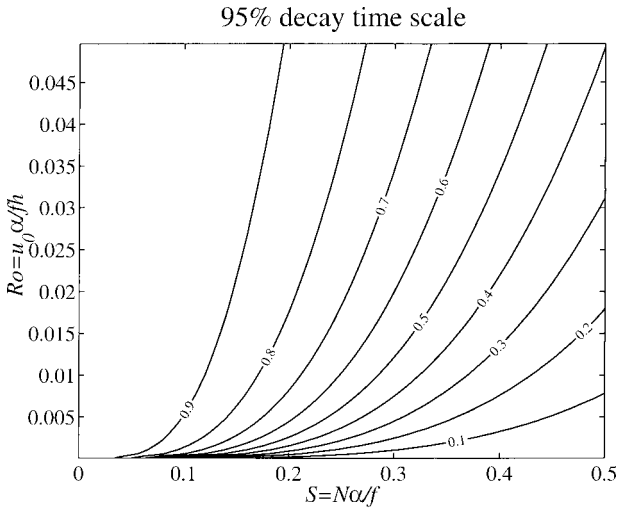

FIG. 4. Contours of the scaled time needed to decelerate 95% of the way to steady state, relative to that for frictional spindown, from the theoretical model for a range of S and Ro.

locity scale U in (2). This ratio appears explicitly in (19) and (20). Figure 5 shows u_s^i and the 95% decay timescale versus T_F/T_B for two choices of Ro. The solid curves were computed by varying S over the range required to produce $0 \le T_F/T_B \le 2$. The dashed curve in Fig. 5a was calculated from (19) after neglecting S^2 compared to unity ($S_2 \ll 1$) and shows that, to a good approximation, u_s^i depends only on the ratio of timescales given by (21). The limit of $T_F/T_B \to 0$ is pure frictional spindown (i.e., the timescale for buoyancy shutdown goes to infinity), and the limit of large T_F/T_B is pure buoyancy shutdown. As expected, u_s^i increases toward unity and the decay timescale decreases toward zero as buoyancy shutdown becomes more important (as T_F/T_B increases). The surprising result is that u_s^i remains large and the decay timescale is substantially reduced even when T_F/T_B is well below one. This means that buoyancy shutdown is still important when its individual timescale (2) is much larger than the frictional timescale (1). For example, when $T_B = 5T_F$, the steady velocity is 46%–48% of its initial value, varying slightly with Ro. The steady velocity does not fall below 25% until $T_B \approx 25T_F$, implying that buoyancy shutdown may be important on much shorter timescales than previously thought.

Another interesting result is that the solution (18) is not nearly as sensitive to stratification or bottom slope as was anticipated from the buoyancy shutdown timescale (2). In fact, for small S, (19) shows that $u_s^i \approx S^2(2/\mathrm{Ro})^{1/2}$, and the sensitivity to S decreases further as S increases. So, applying the results to oceanic conditions may not be as problematic as suggested by (2).

Finally, one of the strengths of the theoretical model is that the simple turbulence closure scheme assumed (i.e., complete vertical mixing of density in the bottom mixed layer) does not require a prescription of the form of τ^x and D in (3) and (7), respectively. Therefore, the results do not depend on estimates of vertical eddy diffusivities and viscosities. The drawback is that part of the solution remains undetermined. For example, it has been shown from continuity (6) that the depth-integrated cross-isobath velocity must vanish at all times. According to (3), the steady interior cross-isobath velocity v^i vanishes because there is no stress above the bottom mixed layer. Therefore, the steady cross-isobath transport in the bottom mixed layer must also vanish (i.e., $\int_{-h}^{-h+\delta} v\, dz = 0$). However, v within the bottom mixed layer depends on the details of the vertical mixing of density and momentum and is not determined in the present model. Indeed, the numerical model results (section 3) show that the way in which cross-isobath transport vanishes in the bottom mixed layer varies considerably with the turbulence closure scheme.

3. Numerical model

Many assumptions were made in deriving the theoretical model of section 2, some of which may be ques-

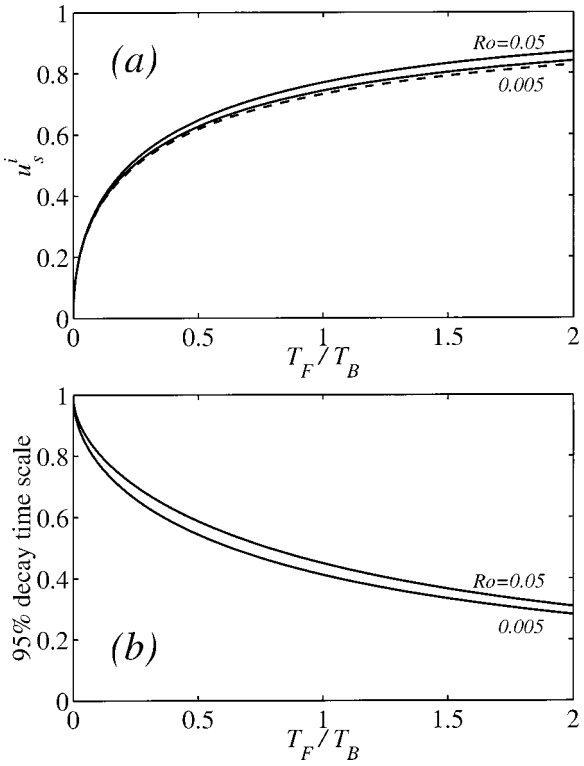

FIG. 5. (a) Steady scaled interior velocity and (b) 95% decay time (as in Fig. 4) vs the ratio of frictional spindown time (1) to buoyancy shutdown time (2) from the theoretical model for two values of Ro. The dashed curve in (a) is an approximate solution when $S^2 \ll 1$ in (19).

tionable in a more realistic scenario. In this section, a primitive-equation numerical model is used to test the validity of the assumptions and the sensitivity of the results within the context of more complete dynamics.

a. Description

The model used here is the well-known *s*-coordinate primitive-equation model (SPEM5.1) developed by D. Haidvogel's group at Rutgers University. Only a brief description of the model is included here. Readers should refer to Haidvogel et al. (1991) and Song and Haidvogel (1994) for details. The following hydrostatic and Boussinesq momentum, density, and continuity equations are solved:

$$u_t + \mathbf{u}\cdot\nabla u - fv = -p_x/\rho_0 + (A_V u_z)_z + F_u \quad (22)$$

$$v_t + \mathbf{u}\cdot\nabla v + fu = -p_y/\rho_0 + (A_V v_z)_z + F_v \quad (23)$$

$$0 = p_z + \rho g \quad (24)$$

$$\rho_t + \mathbf{u}\cdot\nabla\rho = (K_V\rho_z)_z + F_\rho \quad (25)$$

$$u_x + v_y + w_z = 0, \quad (26)$$

where most of the variables have been defined previously. In addition, A_V is the vertical eddy viscosity, K_V is the vertical eddy diffusivity, and $F_{u,v,\rho}$ represent dissipative functions that are required for numerical stability. Subscript x denotes differentiation along the isobaths.

The model domain is a uniformly rotating (f = const) straight channel with solid walls at $y = 0$ and $y = 300$ km. SPEM5.1 is a three-dimensional model, so the two-dimensional calculations are approximated by using a short channel (40 km) with periodic boundary conditions at the open ends ($x = 0$ and 40 km). This does not guarantee perfect two-dimensionality (i.e., $\partial/\partial x$ may not be exactly zero); however, variations in x are extremely small in all of the calculations reported here and can be neglected. The horizontal grid points are uniformly spaced with $\Delta x = 2.2$ and $\Delta y = 2.7$ km.

The bottom is uniformly sloping, with $h = h_c + \alpha y$ where h_c is the shallowest depth and is chosen to make $h = 200$ m at midchannel ($y = 150$ km) where the initial current is centered. In order to resolve the bottom Ekman and mixed layers, grid points are concentrated near the bottom with the s coordinate mapping

$$z(s) = h_c s + (h - h_c)\left\{\frac{\sinh[\theta(s+1)]}{\sinh\theta} - 1\right\}, \quad -1 \le s \le 0, \quad (27)$$

where θ is a prescribed constant, taken as 3.5 for the present calculations. With 30 grid points in the vertical, the grid spacing at the center of the channel ranges from $\Delta z = 2.7$ m at the bottom to $\Delta z = 17$ m at the surface with 7 points within 20 m of the bottom.

There are no fluxes of density or momentum at the surface or the solid sidewalls. At the bottom, the density flux is zero, while the shear stress is specified using a linear bottom friction parameterization,

$$A_V u_z = ru; \qquad A_V v_z = rv \qquad \text{at } z = -h, \quad (28)$$

where r is the previously defined bottom friction coefficient.

The vertical mixing coefficients are approximated using a Richardson-number-dependent scheme:

$$A_V = 10^{-6} + \frac{10^{-2} - 10^{-6}}{(1.0 + 0.3\mathrm{Ri})^{1/2}} \quad (29)$$

$$K_V = 10^{-6} + \frac{10^{-2} - 10^{-6}}{(1.0 + 0.3\mathrm{Ri})^{3/2}}, \quad (30)$$

where units are $m^2\ s^{-1}$, and the Richardson number is defined by $\mathrm{Ri} = N^2/[(u_z)^2 + (v_z)^2]$. Thus, the mixing coefficients range from $10^{-6}\ m^2\ s^{-1}$ to $10^{-2}\ m^2\ s^{-1}$. The minimum value is an attempt to reduce the leakage of momentum and buoyancy through the top of the bottom mixed layer (Middleton and Ramsden 1996). The maximum value allows a relatively thick Ekman layer that can be resolved more easily, but also results in the need to evaluate the vertical mixing terms implicitly to avoid greatly reducing the time step. Some calculations are made with the Mellor–Yamada level 2 turbulence closure

scheme and will be presented for comparison. However, the resulting values of A_V and K_V are sometimes noisy and sensitive to the time step, so (29) and (30) are generally used. Overall, the results for a downwelling current are not highly sensitive to the choice turbulence closure scheme, but the upwelling cases described in section 3c(2) are quite sensitive. Additional vertical mixing of density is applied in the form of instantaneous convective adjustment whenever the water column becomes statically unstable (i.e., when lighter water appears under heavier water). In the present calculations, this occurs only within the bottom mixed layer.

For numerical stability, Laplacian subgrid-scale mixing with constant mixing coefficients is applied along horizontal surfaces (i.e., $F_{u,v,\rho} = \nu_{u,v,\rho}\nabla^2 u, v, \rho$), using the smallest mixing coefficients that produce stable calculations; $\nu_{u,v} = 50$ m^2 s^{-1} and $\nu_\rho = 10$ m^2 s^{-1}.

In accordance with the theoretical model, each calculation begins with a uniform current with finite width, $u = u_0 = 0.1$ m s^{-1} for 108 km $< y <$ 193 km ($u_0 = -0.1$ m s^{-1} for the upwelling cases). The model is then allowed to run for 30 days of simulation time. The time step is typically 432 s, although some cases require smaller time steps for stability.

b. Flat bottom

To isolate the effects of stratification on frictional spindown, with no possibility of buoyancy shutdown, a preliminary set of calculations was made with a flat bottom ($\alpha = 0$, so $S = \text{Ro} = 0$) and various buoyancy frequencies. Without a sloping bottom, lateral advection of density in the bottom mixed layer does not produce horizontal density gradients. Thus, there is no thermal wind shear in the bottom mixed layer, so buoyancy shutdown cannot occur. Clearly, the basic assumptions of the theoretical model are violated and it cannot apply to the flat bottom case. Momentum terms that were neglected in the theory (e.g., τ^y_z) must become important. In each calculation, $h = 200$ m, $f = 10^{-4}$ s^{-1}, and $r = 5 \times 10^{-4}$ m s^{-1}.

In the absence of stratification, the current decelerates purely by frictional spindown, as described in the introduction. An Ekman layer forms beneath the current with narrow regions of Ekman suction and pumping at the edges that generate strong vertical velocities in the interior, which decrease linearly from the bottom to the surface. There is virtually no vertical shear above the Ekman layer, so the entire interior current slows uniformly.

Stratification modifies deceleration in two important ways. First, the vertical mixing coefficients are altered such that mixing is confined near the bottom. If A_V and K_V were constants, then stratification would have little effect on the bottom Ekman layer (Pedlosky 1987). However, the turbulence closure scheme (29) and (30), or any other reasonable scheme, tends to produce large mixing coefficients where the vertical shear is large and/or stratification is weak, and small values where shear is small and/or stratification is strong. Therefore, in the present calculations, A_V and K_V are large near the bottom and small in the interior. This produces a bottom mixed layer with height proportional to $u_*/(fN)^{1/2}$ where $u_* = (\tau^x/\rho_0)^{1/2}$ is the bottom friction velocity (Weatherly and Martin 1978). Stronger stratification leads to a thinner bottom mixed layer, with larger v (to accomodate the same Ekman transport), and consequently stronger vertical velocities into and out of the interior at the current edges. Thus, the vertical velocity should be inversely proportional to bottom mixed layer thickness, that is, $w \sim N^{1/2}$. However, stratification inhibits vertical motions, and the vertical scale of penetration is proportional to f/N. Taken together, the influence of the vertical velocity on the interior should be proportional to $N^{-1/2}$, with the net result that stronger stratification should reduce the transmission of bottom stress to the interior fluid and slow the deceleration process.

The second impact of stratification is that the vertical velocities produced by Ekman suction and pumping at the current edges produce vertical advection of density, which lowers and raises interior isopycnals. This leads, through thermal wind, to vertical shears of the interior velocities that reduce the velocity near the bottom, thereby reducing the bottom stress and further decoupling the interior flow from the bottom mixed layer.

Figure 6 shows vertical sections of u and ρ after 15 days of deceleration with $N = 0$, 0.005, and 0.02 s^{-1}. The features described above are evident. The bottom mixed layer is thinner by about a factor of 2 when N is larger by a factor of 4, consistent with the $N^{-1/2}$ scaling. Sloping interior isopycnals are obvious in Fig. 6b. Stronger stratification requires smaller isopycnal slopes to produce large interior shears, and Fig. 6c shows that the near-surface flow is quite different from that just above the bottom mixed layer. The interior flow has been effectively decoupled from the bottom mixed layer. Note that the current does not widen appreciably in any of these cases, in support of the theoretical model of section 2.

Figure 7 shows the deceleration of the interior current over a flat bottom for several choices of stratification. In all cases, the current decelerates at a slower rate than the theoretical timescale estimate of h/r, the difference being caused by the cross-channel component of bottom stress (τ^y) that was neglected in the theoretical model. The additional bottom stress weakens the cross-channel flow in the bottom boundary layer, which in turn reduces the Ekman suction and pumping and the stress redistribution throughout the water column, leading to slower deceleration. This is consistent with the numerical results of Chapman (2000), who found greatly increased cross-isobath velocities in the bottom boundary layer when τ^y was excluded. The final state was not terribly different, but the adjustment to that state was quite different.

Suprisingly, when stratification is strong, deceleration stops before reaching a state of rest, leaving a nonzero steady current, even without the influence of buoyancy shutdown. In these cases, the initially strong Ekman

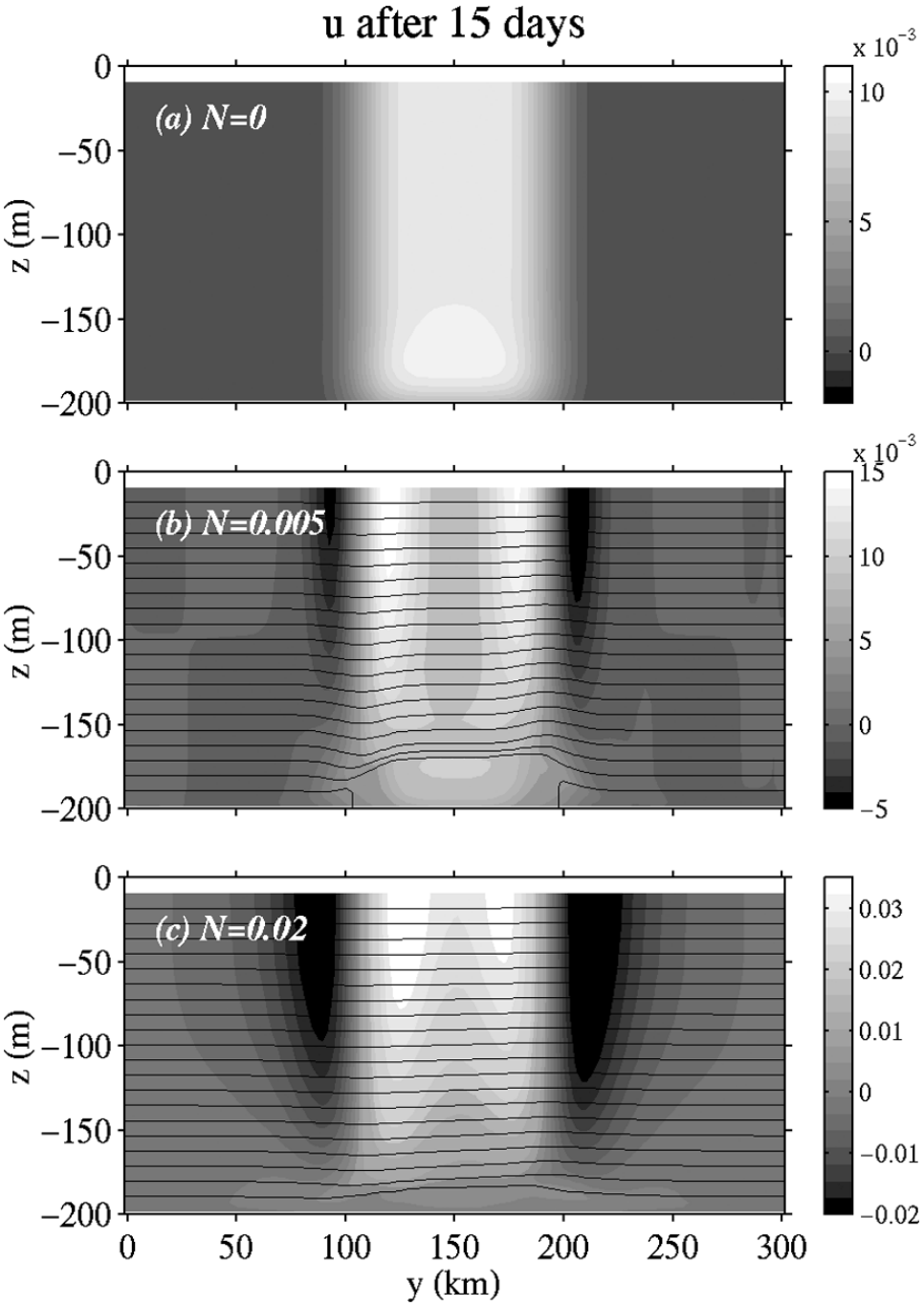

FIG. 6. Vertical sections of u and ρ after 15 days of deceleration over a flat bottom in the numerical model with different stratifications: (a) $N = 0$, (b) $N = 0.005$ s^{-1}, (c) $N = 0.02$ s^{-1}. Other parameters are $u_0 = 0.1$ m s^{-1}, $f = 10^{-4}$ s^{-1}, and $r = 5 \times 10^{-4}$ m s^{-1}. Velocities are given on the bar on the right in m s^{-1}.

suction and pumping produces large vertical shears in the interior velocities, largely decoupling them from the bottom mixed layer. Then bottom stress reduces the velocities in the bottom mixed layer, and hence the Ekman suction and pumping, until the near-surface currents are essentially unaffected by the dynamics within the bottom mixed layer. A complete study of the dynamics of the flat bottom case is beyond the scope of this paper. However, the results suggest that if buoyancy shutdown is to play an important role, it must significantly alter the flat bottom deceleration; for example, it should produce a substantially stronger steady current.

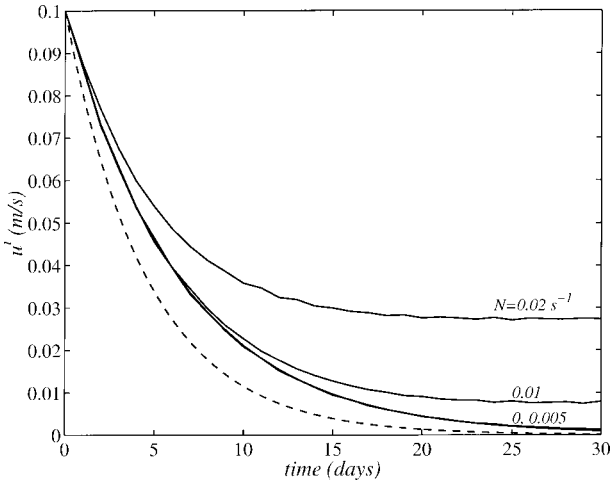

FIG. 7. Along-channel velocity at the surface at the center of the current ($y = 150$ km, $z = 0$) vs time from the numerical model with a flat bottom (see Fig. 6) and various initial stratifications. Parameters are $u_0 = 0.1$ m s^{-1}, $f = 10^{-4}$ s^{-1}, $r = 5 \times 10^{-4}$ m s^{-1}, and $h = 200$ m. The dashed curve is the analytical solution for pure frictional shutdown, $u = u_0 e^{-rt/h}$.

c. Sloping bottom

1) DOWNWELLING CURRENT

A sloping bottom introduces buoyancy shutdown, in addition to the effects of stratification described in the previous subsection. A typical example of the flow produced by the numerical model is shown in Fig. 8 for a bottom slope of $\alpha = 0.001$, with $u_0 = 0.1$ m s^{-1}, $N = 0.01$ s^{-1}, $f = 10^{-4}$ s^{-1}, and $r = 5 \times 10^{-4}$ m s^{-1} ($S = 0.1$, Ro $= 0.005$). After 5 days, the velocities and bottom mixed layer have structures closely resembling the theoretical model (Fig. 1b); the current width is roughly unchanged, and a thick bottom mixed layer has formed with nearly vertical isopycnals. Flow in the bottom mixed layer is downslope, with a weak return flow over most of the interior ($v^i < 0$). In addition, the interior isopycnals have been altered by vertical advection to produce interior vertical shears, as in the flat bottom case. After 20 days, the bottom mixed layer is slightly thicker, the interior cross-isobath velocity v^i has nearly vanished, and the along-isobath velocity is nonzero in the interior but nearly zero at the bottom. The flow has basically reached a steady state. These features are typical of the numerous numerical calculations made here using a variety of parameter combinations.

Figure 9 shows a comparison between the theoretical and numerical models at the center of the current. The bottom mixed layer thickness in the numerical model δ_n is estimated by the depth range over which the bottom density isopycnal ρ^b must have moved from its original position. Using (9),

$$\delta_n = h - g\rho^b/\rho_0 N^2. \tag{31}$$

The agreement between numerical model and theory is quite good in this case. The initial deceleration is slower in the numerical model owing to the presence of the cross-isobath stress term, as noted above in the flat bottom calculations. This reduces the vertical shear of the along-isobath velocity in the bottom mixed layer, so a slightly thicker (by about 2 m) bottom mixed layer is required in the numerical model to bring the bottom velocity to zero.

The cross-isobath structure of the theoretical and numerical steady-state solutions is shown in Fig. 10. The solutions have roughly the same magnitudes, but the numerical model exhibits considerably more structure in the surface velocity. This results primarily from the sloping interior isopycnals and consequent vertical shear discussed in the flat bottom cases. There is also a reversal in u^i at the current edges, again caused by the tilted isopycnals that produce vertical shear of the opposite sign as they approach their resting levels away from the current. The bottom mixed layer thickness is smoother in the numerical model because the edges of the current are more complicated than assumed in the theoretical model. Overall, the numerical model structure lends support to the theory.

In general, the steady states for the numerical calculations agree fairly well with the theoretical model. Figure 11 shows steady states from a variety of numerical calculations with different initial velocities ($u_0 = 0.05$, 0.1, 0.15 m s^{-1}), stratifications ($N = 0$, 0.005, 0.01, 0.015, 0.02, 0.025 s^{-1}), bottom slopes ($\alpha = 0.0005$, 0.001), Coriolis parameters ($f = 0.5$, 1×10^{-4} s^{-1}), and bottom friction coefficients ($r = 0.0005$, 0.001). The solid lines represent perfect agreement. Most velocities fall close to the theoretical estimates. The points at the largest velocities are those with the strongest stratifications. Those points farthest above the solid line are for a gentler bottom slope. In these cases, the interior vertical shear decouples the surface velocity from the deeper velocities (as in the flat bottom cases), so buoyancy shutdown is more effective and produces a larger steady velocity. The numerical model typically produces a thicker bottom mixed layer than the theory suggests, but the parameter dependences (i.e., the trend of the circles) agree reasonably well. The point farthest from the line on the δ_s plot is for weak stratification ($N = 0.005$ s^{-1}) and gentle bottom slope ($\alpha = 0.0005$), which is closest to the flat bottom case, and δ_s is set more by the stratification limitation than by buoyancy shutdown.

Evaluation of individual terms in the momentum and heat balances (22)–(25) shows that the nonlinear momentum terms, lateral subgridscale mixing ($F_{u,v,\rho}$), and variations in x are all negligibly small (not shown). Furthermore, within the bottom mixed layer, the local along-isobath acceleration (u_t) in (22) is much smaller than either the Coriolis or stress terms, justifying its neglect in the theoretical model to obtain (12). The only term that was neglected in the theoretical model but, though small, is not negligibly small in the numerical model is the cross-isobath stress divergence, $\tau^y_z =$

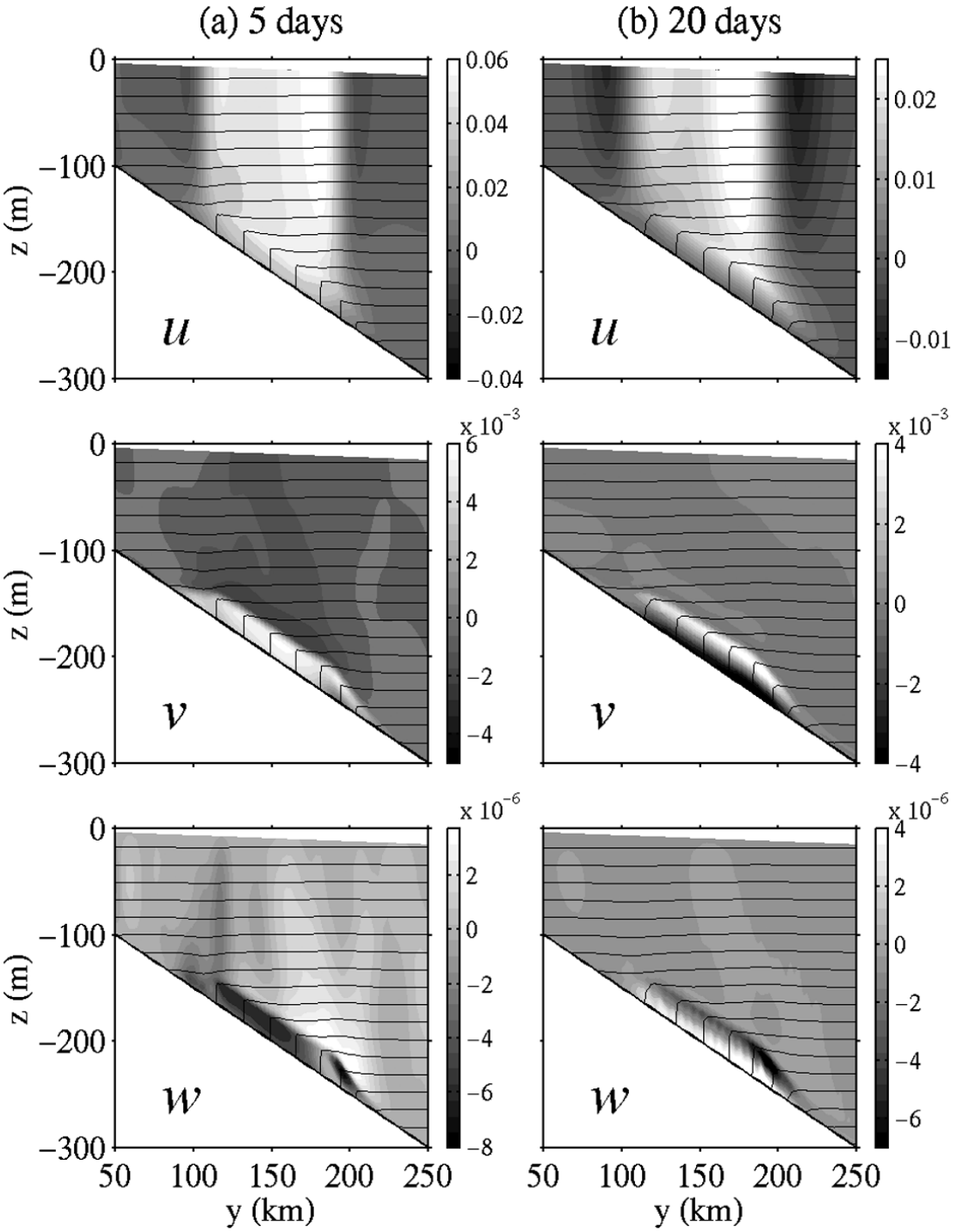

FIG. 8. Vertical sections of u, v, and w with ρ superimposed after (a) 5 and (b) 20 days of deceleration over a bottom slope of $\alpha = 0.001$ in the numerical model. Other parameters are $N = 0.01\ \text{s}^{-1}$, $u_0 = 0.1\ \text{m s}^{-1}$, $f = 10^{-4}\ \text{s}^{-1}$, and $r = 5 \times 10^{-4}\ \text{m s}^{-1}$. Velocities are given on the bar on the right in m s^{-1}.

$(A_V v_z)_z$ in (23). As noted in the flat bottom calculations, the cross-isobath stress reduces v in the bottom mixed layer, which reduces Ekman suction and pumping at the current edges and slows deceleration (Fig. 7).

Another consequence of the cross-isobath stress is to produce steady-state velocities that fall below the theoretical estimates; the disagreement generally increases as the stratification increases (Fig. 12). The reason is that buoyancy shutdown only reduces the along-isobath velocity to zero at the bottom, not the cross-isobath

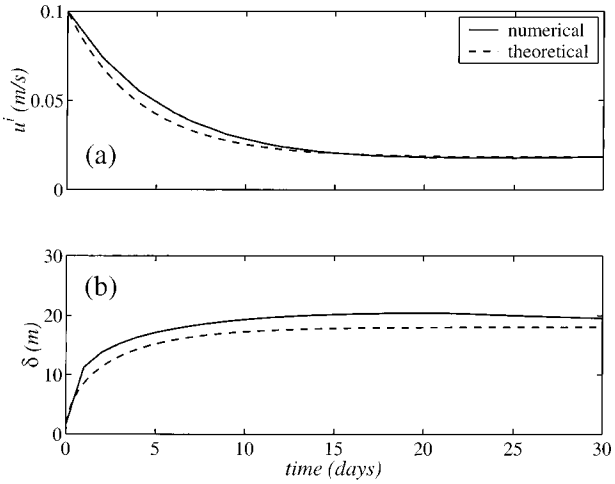

FIG. 9. Comparison of the approach to steady state for the numerical and theoretical models. Solid curves are (a) surface velocity and (b) bottom mixed layer thickness estimated from (31), each at the center of the current in the numerical calculation shown in Fig. 8 with $\alpha = 0.001$, $N = 0.01\ \mathrm{s}^{-1}$, $u_0 = 0.1\ \mathrm{m\ s}^{-1}$, $f = 10^{-4}\ \mathrm{s}^{-1}$, and $r = 5 \times 10^{-4}\ \mathrm{m\ s}^{-1}$. Dashed curves are the equivalent theoretical quantities plotted as unscaled variables using the same parameters.

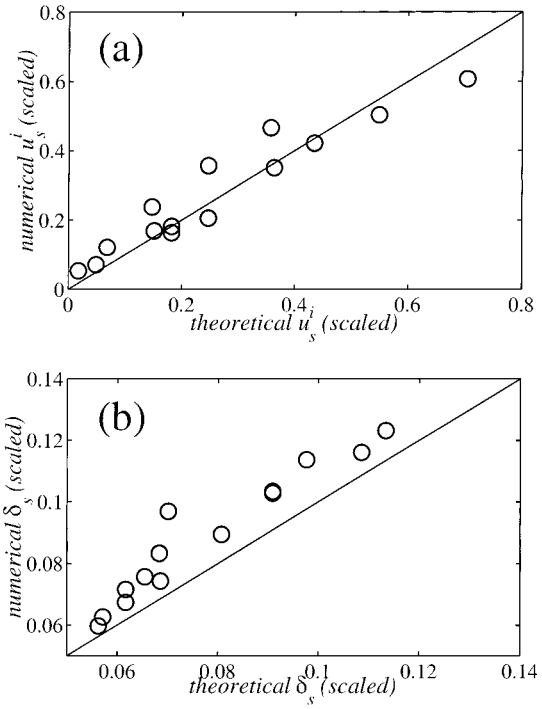

FIG. 11. Comparison of steady scaled (a) interior velocity and (b) bottom mixed layer thickness from theoretical and numerical models using a variety of parameter combinations (see text for details). Numerical values of u_s^i are taken at the surface at the center of the current. Solid lines indicate perfect agreement.

velocity. Therefore, cross-isobath stress may remain and be substantial even after the along-isobath stress vanishes. Figure 13 shows both components of the bottom velocity, u^b and v^b, for three stratifications. In all three cases, $u^b \to 0$ smoothly and remains close to zero. On the other hand, v^b passes through zero and stays negative for the remainder of each calculation. The magnitude of v^b increases with increasing N, so the current continues to decelerate despite the fact that buoyancy shutdown has arrested the along-isobath velocity.

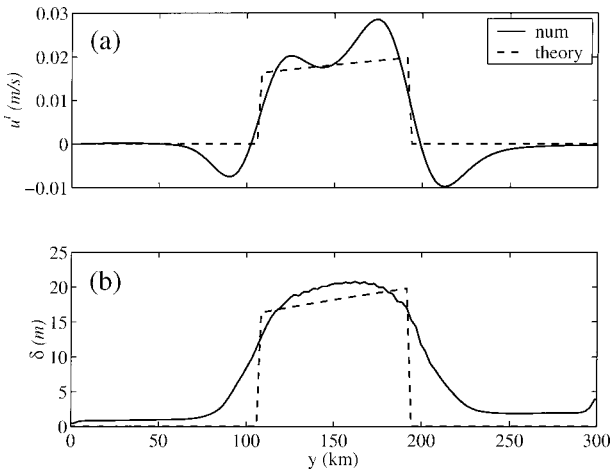

FIG. 10. Comparison of cross-isobath structures for the numerical and theoretical models. Solid curves are (a) surface velocity and (b) bottom mixed layer thickness estimated from (31), from the numerical calculation shown in Fig. 8b with $\alpha = 0.001$, $N = 0.01\ \mathrm{s}^{-1}$, $u_0 = 0.1\ \mathrm{m\ s}^{-1}$, $f = 10^{-4}\ \mathrm{s}^{-1}$, and $r = 5 \times 10^{-4}\ \mathrm{m\ s}^{-1}$. Dashed curves are the equivalent theoretical quantities plotted as unscaled variables using the same parameters.

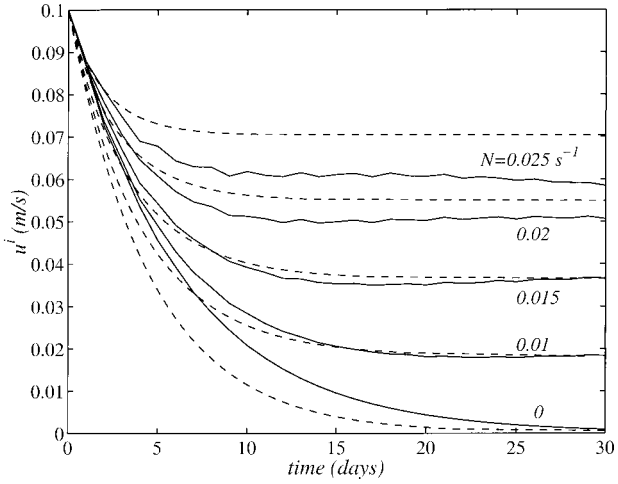

FIG. 12. Comparison of deceleration of the interior velocity for the numerical and theoretical models. Solid curves are the surface velocities at the center of the current from the numerical model using different buoyancy frequencies. Other parameters are $\alpha = 0.001$, $u_0 = 0.1\ \mathrm{m\ s}^{-1}$, $f = 10^{-4}\ \mathrm{s}^{-1}$, and $r = 5 \times 10^{-4}\ \mathrm{m\ s}^{-1}$. Dashed curves are the equivalent theoretical (unscaled) interior velocities using the same parameters.

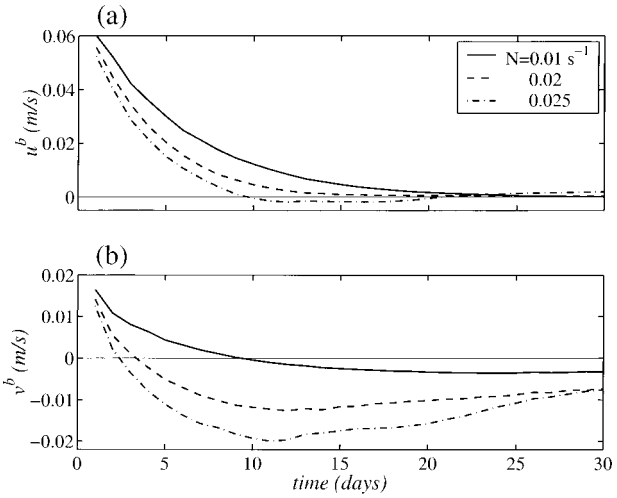

FIG. 13. Time histories of (a) along-isobath bottom velocity u^b and (b) cross-isobath bottom velocity v^b, measured at the center of the current, from the numerical model using several different buoyancy frequencies. Other parameters are $\alpha = 0.001$, $u_0 = 0.1$ m s^{-1}, $f = 10^{-4}$ s^{-1}, and $r = 5 \times 10^{-4}$ m s^{-1}.

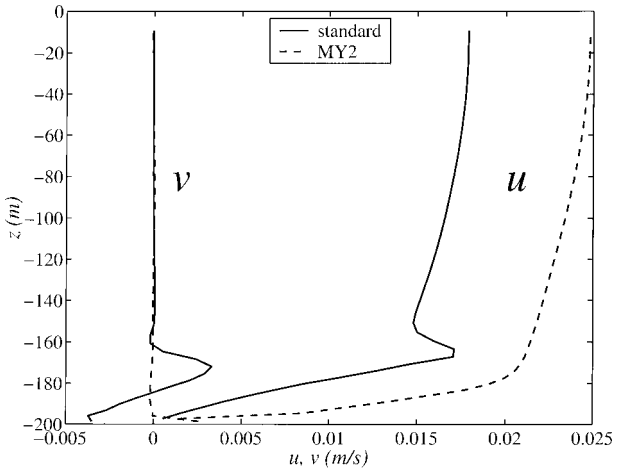

FIG. 14. Vertical profiles of u and v at the center of the current ($y = 150$ km) from the numerical model after 25 days of deceleration and for different turbulence closure schemes. Solid curves are for the standard mixing scheme (29) and (30). Dashed curves are for the Mellor–Yamada level 2 scheme. Parameters are $\alpha = 0.001$, $N = 0.01$ s^{-1}, $u_0 = 0.1$ m s^{-1}, $f = 10^{-4}$ s^{-1}, and $r = 5 \times 10^{-4}$ m s^{-1}.

The reversal in the cross-isobath bottom velocity is part of the strong cross-isobath circulation within the bottom mixed layer in Fig. 8b. This circulation is present in every calculation presented thus far. As discussed in section 2, the cross-isobath *transport* in the bottom mixed layer must vanish in steady state, but the cross-isobath *velocity* need not vanish. Instead of vanishing, Fig. 8b shows that the cross-isobath flow is upslope near the bottom and downslope in the upper part of the bottom mixed layer. Surprisingly, this flow pattern is a result of the turbulence closure scheme. Once the bottom mixed layer is established, the mixing coefficients computed from (29) and (30) are always at their maximum within the bottom mixed layer (i.e., $\rho_z \approx 0$, so Ri ≈ 0 there). As $u^b \to 0$ in (28), the along-isobath bottom stress $A_V u_z$ can then only vanish by $u_z \to 0$, and not by a reduction of the mixing coefficient at the bottom. Within most of the bottom mixed layer, thermal wind dictates that $u_z \approx \alpha N^2/f > 0$, so as steady state is approached, u_z at the bottom is less than the thermal wind shear. Thus, $(A_V u_z)_z > 0$ near the bottom, which requires $v < 0$ in the x-momentum equation (22). (Remember that all other terms are small in the two-dimensional, steady state.) The stress divergence has opposite sign at the top of the bottom mixed layer, so $v > 0$ there. The result is the strong recirculation within the bottom mixed layer seen in Fig. 8b and the continued deceleration of the flow. Eventually, this recirculation begins to restratify the bottom mixed layer, but these dynamics are largely a consequence of the particular turbulence closure scheme and are not examined further.

To demonstrate the sensitivity to the turbulence closure scheme, several numerical calculations have been repeated using the Mellor–Yamada Level 2 (MY2) scheme for comparison with the results just described. MY2 also uses the Richardson number for estimating A_V and K_V, but it is based on energy arguments that allow the mixing coefficients to vary in regions where stratification is absent. Thus, A_V can approach zero near the bottom, thereby reducing the bottom stress to zero independent of the vertical shear at the bottom. The cross-isobath circulation in the bottom mixed layer seen in Fig. 8b does not develop (Fig. 14). Instead, v in the bottom mixed layer approaches zero everywhere except at the bottom grid point, and the transition in u at the top of the bottom mixed layer is much smoother. A side effect is that u^b never quite vanishes, which, coupled with nonzero v^b, leads to a slower deceleration that appears not to reach a steady state (Fig. 15). The difference between the two cases increases for stronger stratification. Nevertheless, despite these differences, the effects of buoyancy shutdown are clearly present in all cases.

2) UPWELLING CURRENT

The theoretical model does not address the deceleration of an upwelling current, but this case can be examined using the numerical model simply by changing the sign of u_0. Transport in the bottom Ekman layer is now initially upslope, carrying heavier water under lighter water, which, being stable, does not generate a mixed layer but rather develops a thinning stratified layer near the bottom. The resulting density gradients and thermal wind shear are opposite to the downwelling case, so the interior velocity is still reduced toward the bottom.

Buoyancy shutdown alone under upwelling flows has been studied extensively using one-dimensional models (see the references in the introduction) but again not simultaneously with frictional spindown. One persistent

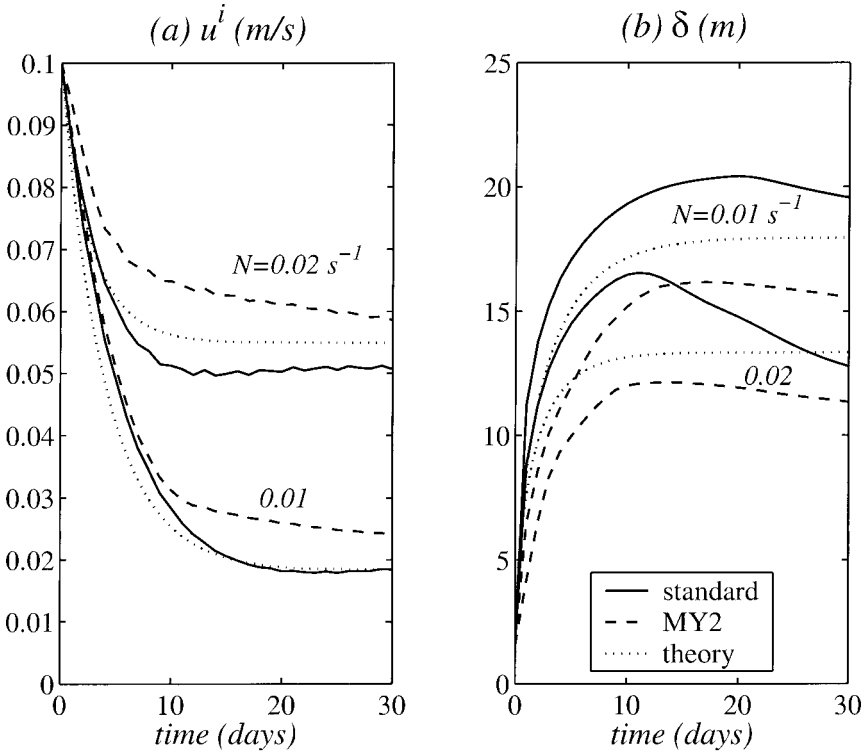

FIG. 15. Time evolution of the (a) surface velocity at the center of the current, and (b) the bottom mixed layer thickness estimated from (31) from numerical model calculations using different turbulence closure schemes. Solid curves are for the standard mixing scheme (29) and (30). Dashed curves are for the Mellor–Yamada level 2 scheme. Dotted curves are the corresponding theoretical solutions using the same parameters. Parameters are $\alpha = 0.001$, $N = 0.01$ s^{-1}, $u_0 = 0.1$ m s^{-1}, $f = 10^{-4}$ s^{-1}, and $r = 5 \times 10^{-4}$ m s^{-1}.

result is that buoyancy shutdown of an upwelling flow occurs faster than for a downwelling flow, so it may be expected that a steady state will be reached for upwelling flows, perhaps more rapidly than for downwelling flows.

Unfortunately, the results are difficult to generalize because they are highly dependent on the turbulence closure scheme. Buoyancy shutdown is active in all cases examined here and can significantly alter deceleration, leading to a steady state with nonzero interior flow and small bottom stress. However, the magnitude and structure of the steady state are quite different when using the two turbulence closure schemes. For example, Fig. 16 shows sections of u and ρ after 20 days of deceleration from an initial velocity of $u_0 = -0.1$ m s^{-1} (with $N = 0.01$ s^{-1}, $\alpha = 0.001$, $r = 5 \times 10^{-4}$ m s^{-1}). The interior current has similar structure in both cases, but is considerably stronger in the MY2 case (Fig. 16b). The bottom mixed layers are noticeably different. A relatively well mixed layer forms at the bottom using the standard mixing scheme, while no such layer forms using MY2. The difference again results from the large mixing coefficients produced by the standard mixing scheme near the bottom, as discussed in the previous subsection.

Using MY2 mixing (Fig. 16b), the thermal wind shear near the bottom is of the sense to slow the interior current toward zero at the bottom, rapidly reducing the effectiveness of bottom stress, that is, buoyancy shutdown. A strong, nearly steady interior current is produced, much the same as the equivalent downwelling flows. In contrast, using the standard mixing scheme (Fig. 16a), the thermal wind contribution to the vertical shear within the bottom mixed layer is of the opposite sign to that needed to bring the bottom velocity to zero, so the vertical shear near the bottom is reduced and the overall effect of buoyancy shutdown is diminished. As a result, bottom stress does not vanish rapidly, and the flow continues to decelerate (Fig. 17). Eventually, the interior flow slows enough that the bottom velocity vanishes despite the reduced vertical shear, and a steady state is reached. However, the final interior velocity is considerably weaker than the equivalent downwelling flows. Nevertheless, deceleration in both cases is slower than pure frictional spindown, indicating that buoyancy shutdown is active.

4. Discussion

The relatively simple model considered here is designed to examine the relative importance of frictional

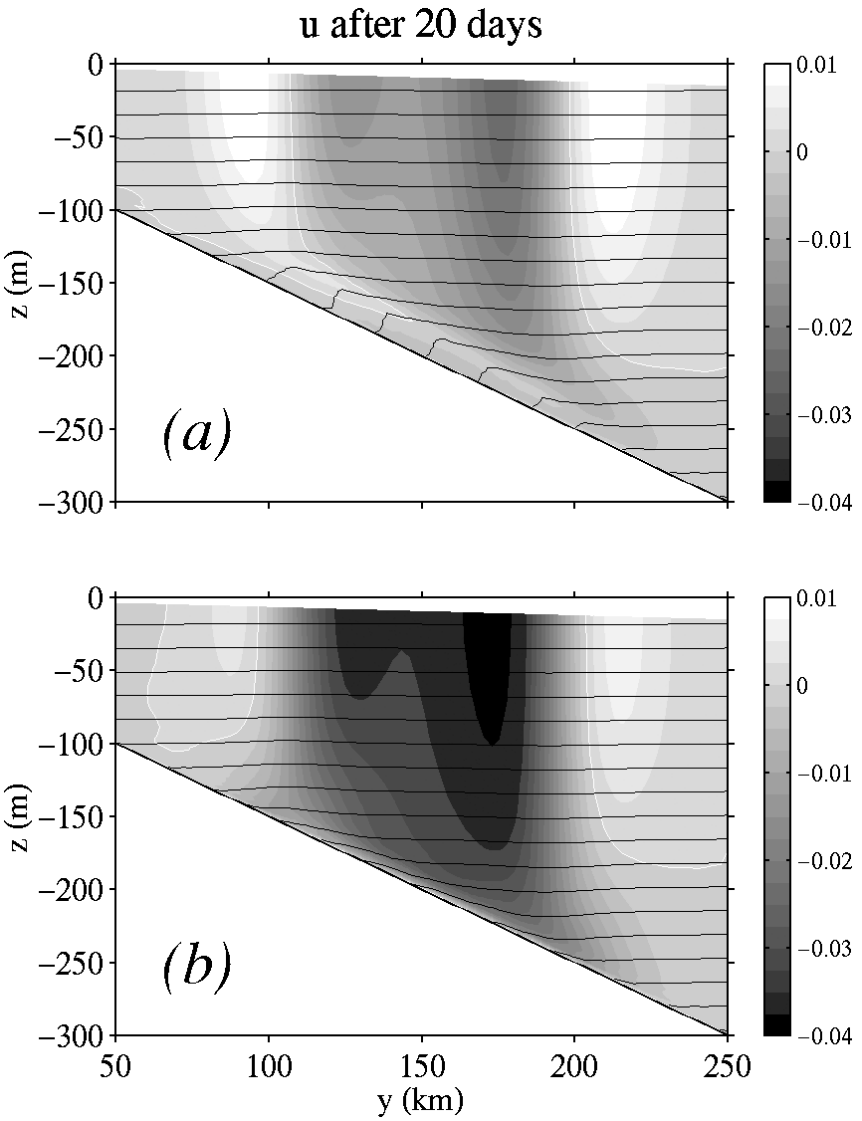

FIG. 16. Vertical sections of u and ρ after 20 days of deceleration from the numerical model with an initially upwelling current ($u_0 = -0.1$ m s^{-1}) using (a) the standard mixing scheme (29) and (30), and (b) the Mellor–Yamada level 2 scheme. Other parameters are $\alpha = 0.001$, $N = 0.01$ s^{-1}, $f = 10^{-4}$ s^{-1}, and $r = 5 \times 10^{-4}$ m s^{-1}. Velocities are given on the bar on the right in m s^{-1}. The white contours are zero velocity.

spindown and buoyancy shutdown on the deceleration of an ocean current. The results show that a simple comparison of timescales for frictional spindown and buoyancy shutdown does not reveal which mechanism dominates the deceleration process. When both mechanisms act simultaneously, buoyancy shutdown always reduces the deceleration timescale from the purely frictional spindown timescale. The change can be substantial, even when the buoyancy shutdown timescale is an order of magnitude longer than for frictional spindown.

Clearly, the present model is idealized and is not intended to represent the complete dynamics of real ocean currents. Many features are ignored that certainly play important roles in the ocean. For example, the two-dimensionality of the model eliminates the possibility that the current may widen due to frictional spreading (e.g., Chapman and Lentz 1997), precludes the effects of alongshelf pressure gradients that may lead to the development of an undercurrent (e.g., Middleton and Cirano 1999), and does not permit alongshelf instabilities. The lack of external forcing (e.g., surface wind stress) limits the current response to deceleration, with no way of maintaining a flow other than the steady flow achieved through buoyancy shutdown. Applying the results to ocean currents is, therefore, problematic.

In addition to these concerns, testing the results with ocean currents is difficult because few existing datasets adequately resolve the vertical structure, both near the

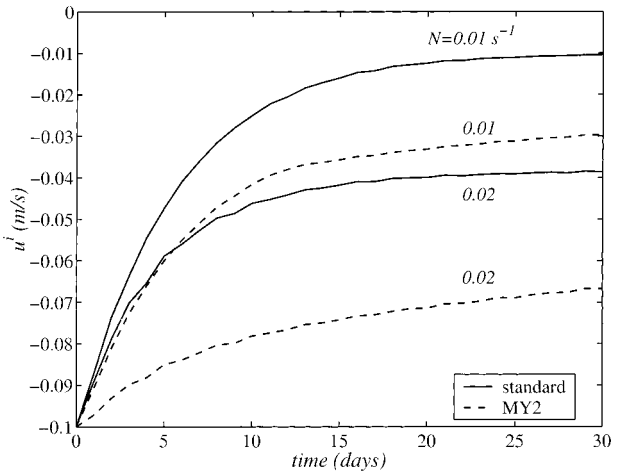

FIG. 17. Time evolution of the surface velocity at the center of the current from the numerical model with an initially upwelling current and different buoyancy frequencies. Solid curves are for the standard mixing scheme (29) and (30). Dashed curves are for the Mellor–Yamada level 2 scheme. Other parameters are $u_0 = -0.1$ m s^{-1}, $\alpha = 0.001$, $f = 10^{-4}$ s^{-1}, and $r = 5 \times 10^{-4}$ m s^{-1}.

bottom and through the water column, to examine the momentum balances for evidence of buoyancy shutdown. An exception is the recent study of currents over the northern California shelf by Lentz and Trowbridge (2001). At a depth of about 90 m, they found strong evidence that buoyancy shutdown influences the current structure and reduces bottom stress on timescales of about one week and greater. The frictional spindown timescale, for $h = 90$ m and $r = 5 \times 10^{-4}$ m s^{-1}, is $T_F = 2.1$ days. This is the *e*-folding decay scale, whereas a current requires three *e*-folding times to decelerate by 95%. That is, the 95% decay time is $3T_F = 6.3$ days. Lentz and Trowbridge (2001) estimated an interior buoyancy frequency in the range $0.004 \text{ s}^{-1} < N < 0.012$ s^{-1}, while $\alpha = 0.005$ and $f = 0.9 \times 10^{-4}$ s^{-1}, leading to a Burger number of $0.22 < S < 0.66$. For a current between 0.1 m s^{-1} and 0.2 m s^{-1}, the Rossby number is $0.06 < \text{Ro} < 0.12$. The theoretical model predicts a reduction from the frictional spindown timescale in the range of 0.23–0.93, depending primarily on the interior stratification. Thus, buoyancy shutdown should be important on timescales of less than 6 days, and possibly even as short as 2 days, although the model is less reliable at high stratifications. The point is that buoyancy shutdown is not limited to its one-dimensional shutdown timescale (2), which would produce estimates of the 95% decay time between 2 and 208 days for the same parameters.

On a broader midlatitude shelf, such as the Middle Atlantic Bight, the buoyancy shutdown timescale is much greater because the bottom slope is considerably smaller, $\alpha \approx 0.001$. For $N = 0.01$ s^{-1}, $f = 10^{-4}$ s^{-1}, and $u_0 = 0.1$ m s^{-1}, the Burger number is $S = 0.1$ and the Rossby number is Ro $= 0.01$; the one-dimensional timescale for buoyancy shutdown from (2) is $T_B = 231$ days (95% decay time of 693 days). This would appear to be much too long to produce an arrested boundary layer. However, the theoretical model predicts a reduction from the frictional 95% decay timescale by a factor of 0.93, so a steady state would be reached in about 6 days, although the steady current would be rather weak. If the stratification were stronger, say $N = 0.02$ s^{-1}, the 95% decay to steady state would take place in about 4.5 days. In general, it appears that buoyancy shutdown may be expected to influence shelf currents on timescales of about 5 days and greater.

Applying these results to deeper regions, for example, the continental slope, is more difficult because currents there are less likely to extend from bottom to surface. Currents such as deep western boundary currents are bottom intensified with strong vertical shears that are not represented by the present model. For example, MacCready (1994) has examined the deceleration of an abyssal current, and he suggests that the decay is caused by Ekman pumping from the bottom boundary layer that gradually drains the momentum from the current by reducing the isopycnal slopes that contain the potential energy of the flow. In his model, the isopycnal slopes are nearly equal to the bottom slope, so buoyancy shutdown is not active. In some sense, this scenario is more like the flat bottom case considered here in which stratification is present, but buoyancy shutdown does not play a role. In addition, recent observations from within the thick bottom mixed layer under a bottom-intensified slope current show no evidence of thermal wind shear, suggesting that the dynamics are different from those modeled here (Stahr and Sanford 1999).

Despite the caveats, it is nevertheless instructive to make rough estimates for flows in deeper regions for comparison to shelf flows. Over the continental slope, the bottom slope and depth both increase dramatically from the shelf values while the stratification generally decreases. If $h = 1000$ m, $\alpha = 0.01$, and $N = 0.001$ s^{-1}, then $S = 0.1$ and Ro $= 0.01$, identical to the broader shelf values. The frictional spindown timescale and the buoyancy shutdown timescale each increase by a factor of 10 to $T_F = 23$ days and $T_B = 2315$ days, respectively. The 95% decay timescale predicted by the theoretical model becomes about 60 days, so the influence of buoyancy shutdown should be limited to much longer timescales than over the continental shelf.

5. Conclusions

The deceleration of an unforced, two-dimensional, finite-width current over a sloping bottom in a stratified fluid has been studied to quantify the relative importance of frictional spindown and buoyancy shutdown when both act simultaneously. A theoretical model of a downwelling current suggests that buoyancy shutdown always reduces the deceleration timescale from that for frictional spindown alone and produces a nonzero steady interior along-isobath current overlying an arrested bot-

tom mixed layer. The steady state is reached more rapidly and the steady current is stronger with increased stratification. Buoyancy shutdown remains important in the deceleration process even when its individual timescale is an order of magnitude larger than the frictional spindown timescale. The model suggests that buoyancy shutdown should influence currents over the continental shelf on timescales of about 5 days and greater.

A primitive-equation numerical model has been used to test the theory and its assumptions. Overall, the results are supportive of the theory, except that the theoretical model neglects the cross-isobath component of bottom stress and ignores vertical shears above the bottom mixed layer. The cross-isobath bottom stress initially slows the deceleration process by reducing Ekman suction and pumping at the edges of the current, but then continues the deceleration after the along-isobath stress has vanished. The result is a weaker steady flow in the numerical model, especially with stronger stratification. Interior vertical shears tend to decouple the near-surface flow from the bottom mixed layer, producing more variable steady flows in the numerical model, depending on the parameter choices.

Details of the flow in the bottom mixed layer are highly dependent on the choice of turbulence closure scheme. If the mixing coefficients cannot approach zero near the bottom, then a strong recirculation develops within the bottom mixed layer as shutdown is approached. That is, the cross-isobath transport in the bottom mixed layer vanishes, but the velocities do not. This produces additional bottom stress, especially when the stratification is strong, that further decelerates the flow and begins to restratify the density field. If the turbulence closure scheme allows small mixing coefficients near the bottom, then both cross-isobath transport and velocity nearly vanish in the shutdown state. The interior steady-state flows produced using each scheme are similar.

Upwelling currents are briefly considered using the numerical model. Buoyancy shutdown is again important in deceleration, substantially reducing the time to reach steady state. For the same reasons described above, the details of both the deceleration and the steady state vary sharply with the turbulent closure scheme, so generalizations are difficult.

Acknowledgments. Discussions with Steve Lentz and John Trowbridge proved highly valuable and are much appreciated. I also thank Rich Garvine for suggesting several improvements to the manuscript. Financial support was provided by the Physical Oceanography Program of the Office of Naval Research under Grant N00014-97-1-0161.

REFERENCES

Chapman, D. C., 2000: A numerical study of the adjustment of a narrow stratified current over a sloping bottom. *J. Phys. Oceanogr.,* **30,** 2927–2940.

——, and S. J. Lentz, 1997: Adjustment of stratified flow over a sloping bottom. *J. Phys. Oceanogr.,* **27,** 340–356.

Garrett, C., P. MacCready, and P. Rhines, 1993: Boundary mixing and arrested Ekman layers: Rotating stratified flow near a sloping boundary. *Annu. Rev. Fluid Mech.,* **25,** 291–323.

Haidvogel, D., J. Wilkin, and R. Young, 1991: A semi-spectral primitive equation ocean circulation model using vertical sigma and orthogonal curvilinear horizontal coordinates. *J. Comput. Phys.,* **94,** 151–185.

Lentz, S. J., and J. H. Trowbridge, 2001: A dynamical description of fall and winter mean current profiles over the northern California shelf. *J. Phys. Oceanogr.,* **31,** 914–931.

MacCready, P., 1994: Frictional decay of abyssal boundary currents. *J. Mar. Res.,* **52,** 197–217.

Middleton, J. F., and D. Ramsden, 1996: The evolution of the bottom boundary layer on the sloping continental shelf: A numerical study. *J. Geophys. Res.,* **101,** 18 061–18 077.

——, and M. Cirano, 1999: Wind-forced downwelling slope currents: A numerical study. *J. Phys. Oceanogr.,* **29,** 1723–1743.

Pedlosky, J., 1987: *Geophysical Fluids Dynamics.* 2d ed. Springer-Verlag, 710 pp.

Ramsden, D., 1995a: Response of an oceanic bottom boundary layer on a slope to interior flow. I. Time independent interior flow. *J. Phys. Oceanogr.,* **25,** 1672–1687.

——, 1995b: Response of an oceanic bottom boundary layer on a slope to interior flow. I. Time dependent interior flow. *J. Phys. Oceanogr.,* **25,** 1688–1695.

Song, Y., and D. Haidvogel, 1994: A semi-implicit ocean circulation model using a generalized topography-following coordinate system. *J. Comput. Phys.,* **115,** 228–244.

Stahr, F. R., and T. B. Sanford, 1999: Transport and bottom boundary layer observations of the North Atlantic Deep Western Boundary Current at the Blake Outer Ridge. *Deep-Sea Res. II,* **46,** 205–243.

Trowbridge, J. H., and S. J. Lentz, 1991: Asymmetric behavior of an oceanic boundary layer above a sloping bottom. *J. Phys. Oceanogr.,* **21,** 1171–1185.

Weatherly, G. L., and P. J. Martin, 1978: On the structure and dynamics of the oceanic bottom boundary layer. *J. Phys. Oceanogr.,* **8,** 557–570.